Results in Physics 41 (2022) 105948

Contents lists available at ScienceDirect

Results in Physics

journal homepage: www.elsevier.com/locate/rinp

Nonlinear dynamical analysis of drift ion acoustic shock waves in Electron-Positron-Ion plasma with adiabatic trapping

Zeeshan Iqbal [a], H.A. Shah [b], M.N.S. Qureshi [a,*], W. Masood [c,d], Amna Fayyaz [a]

[a] Department of Physics, GC University, 54000 Lahore, Pakistan
[b] Department of Physics, FCC (A Charted University), Ferozepur Road, 54600 Lahore, Pakistan
[c] Department of Physics, COMSATS University Islamabad (CUI), Park Road, Islamabad Capital Territory 45550, Pakistan
[d] National Center for Physics (NCP), Quaid-i-Azam University Campus, Shahdrah Valley Road, Islamabad 44000, Pakistan

A B S T R A C T

Propagation of nonlinear coupled drift ion acoustic shock wave is investigated in an electron–positron-ion (*epi*) plasma in the presence of fully degenerate adiabatically trapped electrons. A novel complex nonlinear equation with fractional nonlinear terms is formulated. Phase plane theory of planar dynamical system is employed to investigate this nonlinear equation of *epi* plasma. The variations in nonlinear periodic orbits (NPO), nonlinear heteroclinic orbits (NHO), time series plots and shock profiles are demonstrated by varying the values of different controlling parameters such as the ratio of positron to electron number density, collisional frequency, magnetic field, drift velocity and angle of propagation. It is seen that a pair of shock structures are obtained – which is the most significant result of this work.

Introduction

Nonlinear wave structures in multi-component plasmas containing electrons, positrons and ions as their constituent species have been actively investigated in a variety of cases. The electron–positron-ion (*epi*) plasmas are abundantly found in nature due to the pair production in high energy phenomena such as dense astrophysical plasmas [1–3], intense laser beam induced plasmas [4], active galactic nuclei [5], solar environment [6] and pulsar magnetospheres [7,8], etc. Such plasmas can also be generated in laboratories [9–11]. In contrast to typical electron–ion (*ei*) plasmas, *epi* plasmas exhibit different behavior as the constituent species have the same charge to mass ratio [12]. The reciprocal of electron/positron characteristic plasma frequency is much greater than the electron–positron pair annihilation time period [13] implying that it is possible to investigate *epi* plasmas on a time scale smaller than the annihilation time. It is also well established in the literature that quantum mechanical effects become relevant in the interiors of astrophysical plasmas which are highly dense and hence degenerate [14–17]. Quantum plasmas have a wide range of direct applications in microelectronics [18], carbon nanotubes, quantum dots and quantum wells [19–21].

An extensive amount of research has been carried out to study the characteristics of nonlinear solitary structures in both the *ei* and *epi* plasmas by employing various theoretical models and numerical simulations in classical and quantum regimes [22–24]. Solitary and shock wave structures are formed due to the interplay of nonlinearity with dispersive and dissipative behaviors of the wave respectively [25]. The ion temperature effect on the large amplitude ion acoustic waves in classical *epi* plasmas was studied initially by Nejoh [26]. It was reported that the upper limit of Mach number tends to increase but the amplitude decreases with the enhancement in temperature. Electromagnetic solitary waves in *epi* plasmas were investigated by Verheest [27] by deriving a vector equivalent of the modified Korteweg-de Vries (mKdV) equation. This equation becomes integrable for the linear polarized case only and its super Alfvenic solitary solutions were found by employing the McKenzie technique [28]. Furthermore, the analytical envelope solitary solutions were also studied for the unmagnetized *epi* plasmas [29,30]. In the domain of unmagnetized quantum *epi* plasmas, the linear and nonlinear characteristics of arbitrary amplitude ion acoustic waves were studied in Ali et al. [31] by obtaining the KdV equation and deriving an energy equation to elucidate the findings. The stability and propagation characteristics of ion-acoustic solitary structures in the presence of transverse perturbations were described in Mushtaq and Khan [32] by using the Quantum Hydrodynamic Model (QHD).

In the past decade or so, nonlinear waves in plasmas have been investigated by employing methods for nonlinear dynamical systems. One of the earliest examples of using nonlinear dynamical analysis to investigate nonlinear plasma waves was given by Samanta et al. [33],

* Corresponding author.
E-mail address: nouman_sarwar@yahoo.com (M.N.S. Qureshi).

https://doi.org/10.1016/j.rinp.2022.105948
Received 7 June 2022; Received in revised form 12 August 2022; Accepted 25 August 2022
Available online 30 August 2022

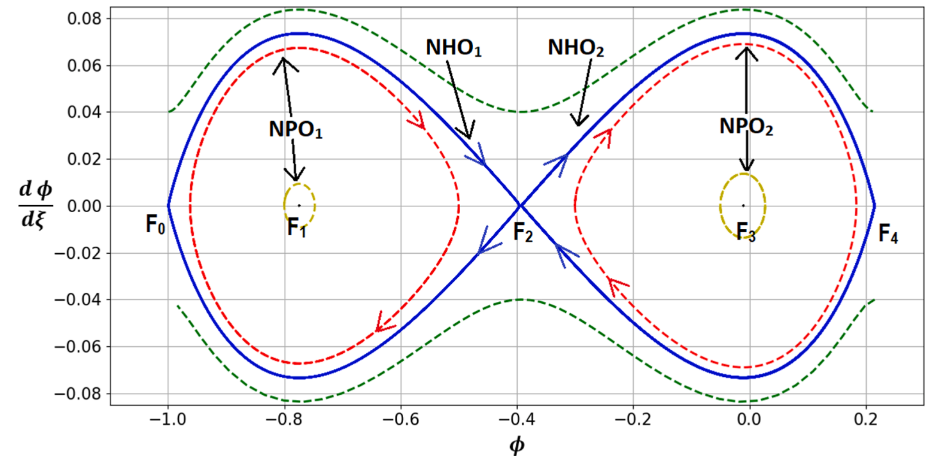

Fig. 1. Phase portrait of the system (16) for $\alpha = 0.1$, $v_{in} = 3\times 10^{13}s^{-1}$, $B_0 = 10^{10}G$, $v_{de} = 0.4$ and $\theta = 60^{\circ}$. The blue solid curve lines are the NHOs correspond to the shock profile while red and yellow dashed lines are the NPOs. $F_0(\phi_0,0)$, $F_1(\phi_1,0)$, $F_2(\phi_2,0)$, $F_3(\phi_3,0)$ and $F_4(\phi_4,0)$ are the fixed points of the nonlinear dynamical system (16). (For interpretation of the references to colour in this figure legend, the reader is referred to the web version of this article.)

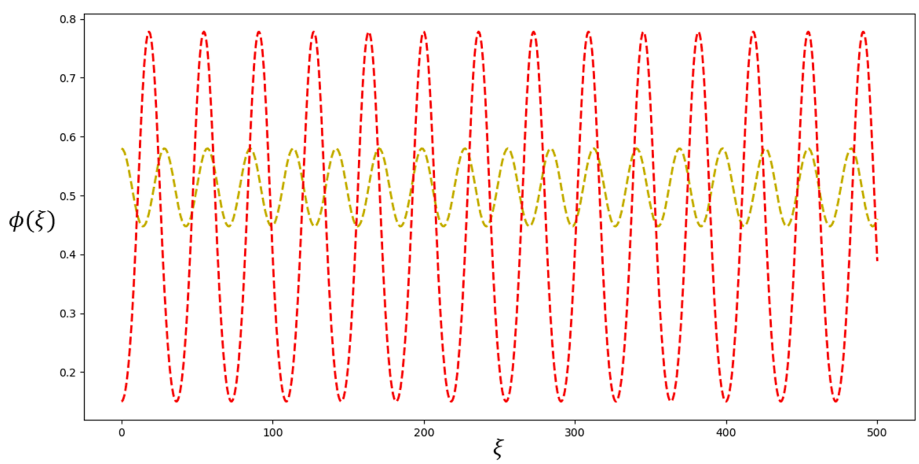

Fig. 2. The time series plots for the NPO_2 with same parameters as used in Fig.-1.

who investigated nonlinear waves in a nonthermal magnetized dusty plasma. Later, these methods were employed for quantum plasmas and the findings were reported in many papers e.g. [34–37]. Nonlinear dynamical methods revealed regions of existence of both solitary structures and nonlinear periodic waves. Recently, Saha [38,39] investigated shock structures of the Burgers equation in dissipative non-extensive e-p-i plasmas. Such an analysis has been applied by El-Monier and Atteya [39] to four component dissipative dusty plasma via the KdV–Burgers (KdVB) equation. More recently, Saha et al. [40] have carried out a bifurcation analysis for kink, anti-kink and periodic waves in dense quantum plasmas. We note here that these methods for plasma physics are well laid out in the recent book by Saha and Banerjee [41].

An important nonlinear phenomenon is that of trapped particles in a stationary electrostatic wave potential which was described by Bernstein et al. [42]. It was shown that there is a crucial dependence of the number density of trapped particles on the generation of solitary structures. Nonstationary adiabatic trapping as a microscopic phenomenon was originally put forward by Gurevich [43] in classical plasmas which gives 3/2 power nonlinearity instead of the usual quadratic nonlinearity in the KdV case. It has also been investigated in various studies that the adiabatically trapped electrons exert a substantial effect on the nonlinear dynamics of degenerate plasmas [44–48]. The effect of the adiabatically trapped electrons in the trough of the slowly varying potential for degenerate plasma was first investigated by Shah et al. [44] which was later extended to study relativistic degenerate plasmas [45]. The generation of vortices has been studied by computing the generalized Hasegawa Mima Equation for scalar and Jacobian nonlinearities concerning electron and positron inhomogeneities [46]. The characteristics of ion acoustic solitary waves have also been investigated under the effects of weak and strong magnetic quantization due to ambient magnetic field [49,50]. Fayyaz et al. have studied the quantum effects of adiabatically trapped electrons in coupled drift ion acoustic shock waves by considering the factual parameters of neutron stars [48]. Later, quantum drift ion acoustic solitary waves have also been investigated and non-linear analysis revealed that inhomogeneity and angle of propagation have a significant effect on solitary structures [47].

In a recent paper [48] (henceforth to be referred to as paper-1), we considered the effect of dissipation in a degenerate inhomogeneous *ei* plasma and obtained a novel Burgers like equation for coupled drift ion acoustic waves, where the nonlinearity was of the form $(1+\phi)^{3/2}$, which yielded an exact shock solution. In the present work, we will investigate the effect of microscopic trapping (adiabatic) in a degenerate inhomogeneous *epi* plasma when dissipation is present via ion-neutral collisions. The inclusion of positrons substantially affects and enriches the results of paper-1 and qualitatively new results appear. We should mention here that shock formation can only be studied numerically in such a plasma, and to this end, we will use the nonlinear dynamical approach. The layout of the paper is as follows: In section 2, we give the mathematical preliminaries. In section 3, we develop the nonlinear

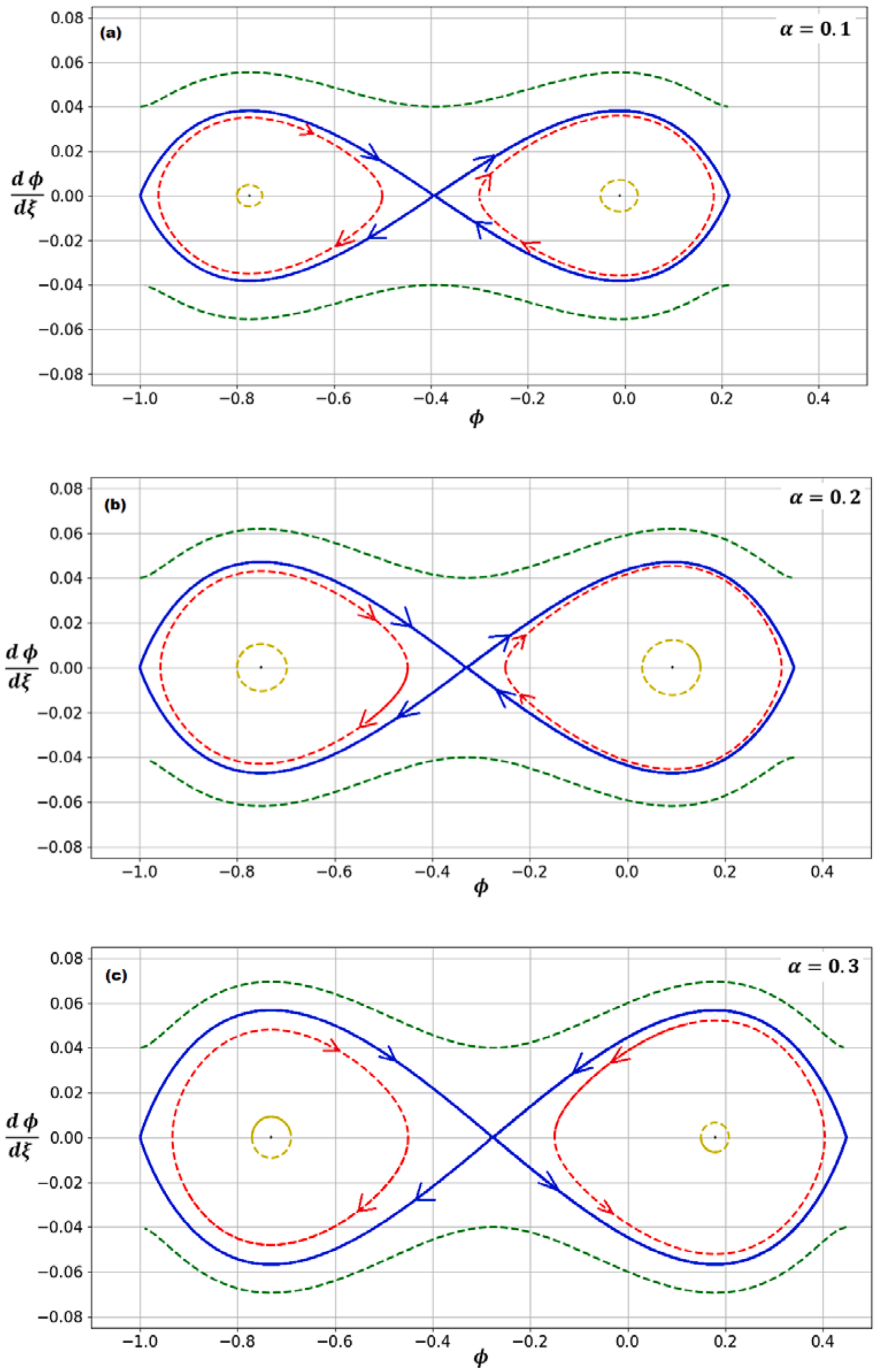

Fig. 3. Phase portrait of the system (16) for different values of $\alpha = 0.1, 0.2$ and 0.3. The other parametric values are $\upsilon_{in} = 3\times10^{13}s^{-1}$, $B_0 = 10^{10}G$, $\nu_{de} = 0.4$ and $\theta = 60^{\circ}$. Three different phase portraits for different values of α and in these phase portraits the blue solid curve lines are the NHOs correspond to the shock profiles while red and yellow dashed lines are the NPOs. (For interpretation of the references to colour in this figure legend, the reader is referred to the web version of this article.)

evolution equation and in section 4, we present the nonlinear dynamical analysis extending the results of paper-1, and in section 5, we use the nonlinear dynamical approach to show numerically how a shock wave is obtained. Finally, in section 6, we give our conclusions about the formation of shock waves.

Basic set of mathematical equations

As stated earlier, we are interested in looking at drift ion acoustic waves in the presence of adiabatic trapping in a quantum *epi* magnetoplasma, where ions are treated as classical due to their heavy mass. The plasma is considered to be collisional, and the external magnetic field B_0 is taken to be in the z-direction whereas the propagation of the wave is considered in the y-z plane and the density inhomogeneity is considered in the x-direction. The quasi-neutrality condition is given as follows

$$n_{e0}(x) = n_{p0}(x) + n_{i0}(x), \tag{1}$$

where, n_{i0}, n_{p0} and n_{e0} are the equilibrium number densities of the ions,

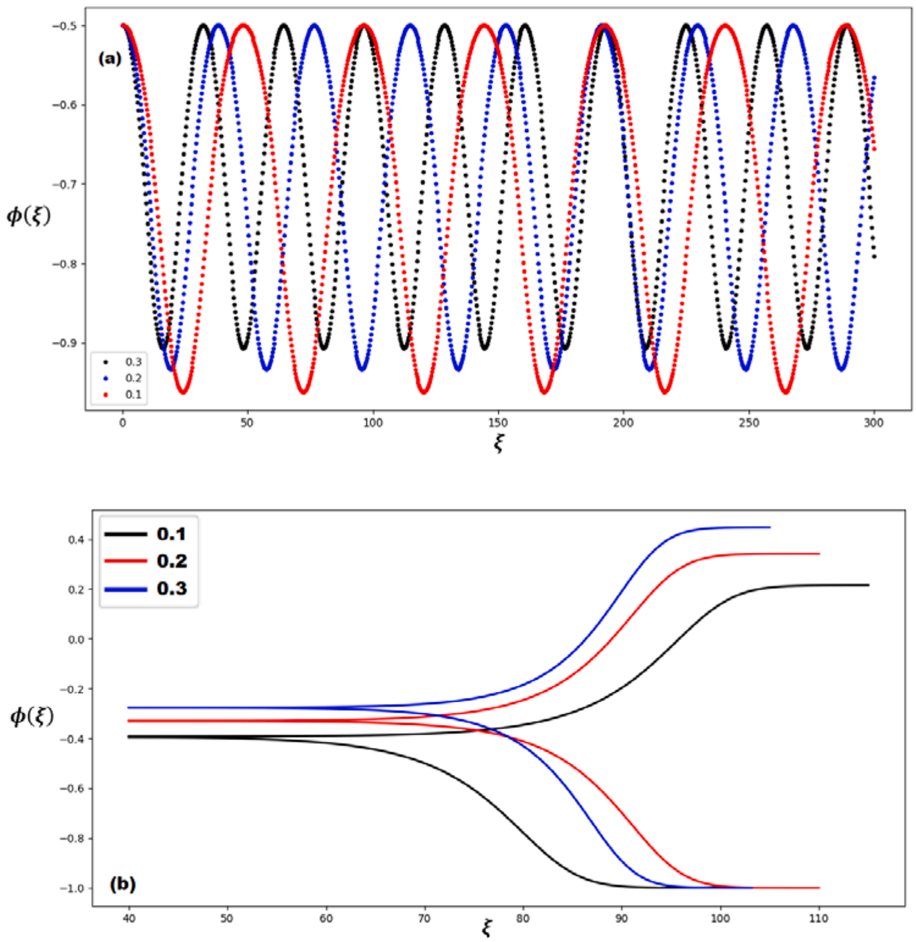

Fig. 4. Time series plots (Fig. 4(a)) and the pair of shock profiles (Fig. 4(b)) of the system (20) for different value of $\alpha = 0.1, 0.2$ and 0.3. The values of other parameters are $\upsilon_{in} = 3\times 10^{13} s^{-1}$, $B_0 = 10^{10} G$, $v_{de} = 0.4$ and $\theta = 60^{\circ}$. The time series plots correspond to the red dashed line of NPO_2 in Fig. 4 while the pair of shock profiles correspond to the blue solid line of NHO_1 and HNO_2 in Fig. 3. (For interpretation of the references to colour in this figure legend, the reader is referred to the web version of this article.)

positrons, and electrons respectively. For low frequency drift ion acoustic waves, the electrons and positrons are considered massless and follow the Fermi Dirac distribution function. Following the method of our earlier papers [44,47,51], we have for the electrons and positrons the following expressions of number densities respectively, which take into account the effect of adiabatic trapping.

$$n_p = n_{p0}\left(1-\frac{e\varphi}{\varepsilon_{Fp}}\right)^{3/2} + n_{p0}T_p^2\left(1-\frac{e\varphi}{\varepsilon_{Fp}}\right)^{-1/2}, \tag{2}$$

$$n_e = n_{e0}\left(1+\frac{e\varphi}{\varepsilon_{Fe}}\right)^{3/2} + n_{e0}T_e^2\left(1+\frac{e\varphi}{\varepsilon_{Fe}}\right)^{-1/2}. \tag{3}$$

Here, n_e (n_p) denotes the total number density of electrons (positrons), T_e (T_p) is the electron (positron) ambient temperatures, φ is the electrostatic potential, e is the charge of an electron, ε_{Fp} and ε_{Fe} are the positron and electron Fermi energies, respectively and are considered in standard form as $\varepsilon_{Fp,Fe} = \frac{\hbar^2}{2m_{p,e}}(3\pi^2 n_{p0,e0})^{2/3}$. In our calculations, we will consider a fully degenerate plasma, thus $T_{p,e}$ are taken to be zero. In the case of the zero-temperature limit, the chemical potentials in the Fermi–Dirac distribution function is $\mu_{e,p} = \varepsilon_{Fp,Fe}$.

The ions on the other hand are taken to be classical, which is justified since $m_i \gg m_{e,p}$ and thus quantum mechanical effects for the ions are taken to be negligible. We also consider the ions to be cold as in most cases of interest and temperature in energy units is $T_i \ll \varepsilon_{Fp,Fe}$. Using the standard drift approximation [52], the following expression for the perpendicular and parallel components of the ion velocities are obtained, respectively.

$$v_{i\perp} = -\frac{c}{B_0}\left(\frac{\partial\varphi}{\partial y}\widehat{x} + \frac{\partial\varphi}{\partial x}\widehat{y}\right) - \frac{c}{B_0\omega_{ci}}\frac{\partial}{\partial t}\frac{\partial\varphi}{\partial y}\widehat{y} - \frac{c\upsilon_{in}}{B_0\omega_{ci}}\frac{\partial\varphi}{\partial y}\widehat{y}, \tag{4}$$

$$\widehat{A}v_{i\parallel} = -\frac{e}{m_i}\frac{\partial\varphi}{\partial z}. \tag{5}$$

Here, $v_{i\perp}$ is the perpendicular component of ion velocity in the plane perpendicular to the ambient magnetic field B_0, υ_{in} is the ion neutral collisional frequency and $\omega_{ci} = \frac{eB_0}{m_i c}$ is the ion gyro frequency, here m_i is the ion mass and c is the velocity of light. The right hand side of Eq. (4) represents the different drift velocities, the first term is the dominant $E\times B$ drift, second term represents the polarization drift and the last term is the collisional drift. The operator $\widehat{A}$ is given by $\widehat{A} = \frac{\partial}{\partial t} + \upsilon_E \bullet \nabla_\perp + v_{i\parallel}\frac{\partial}{\partial z}$ and $v_{i\parallel}$ is the parallel ion velocity. We note here that these are standard results from the drift approximation theory [52] and hence have not been derived here. For the sake of completeness, we give here the equation of continuity for ions.

$$\frac{\partial n_i}{\partial t} + n_i(\nabla\bullet v_i) + v_i\bullet(\nabla n_i) = 0, \tag{6}$$

and Poisson's equation which is given by

$$\nabla^2\phi = -4\pi e\left(n_i + n_p - n_e\right), \tag{7}$$

where, $\phi = e\varphi/\varepsilon_{Fe}$ is the normalized potential.

Now, following our earlier work [48] and using Eqs. (1)–(5) and substituting these in Eq. (6), we obtain the following nonlinear evolution equation, in dimensionless form, for collisional drift ion acoustic waves.

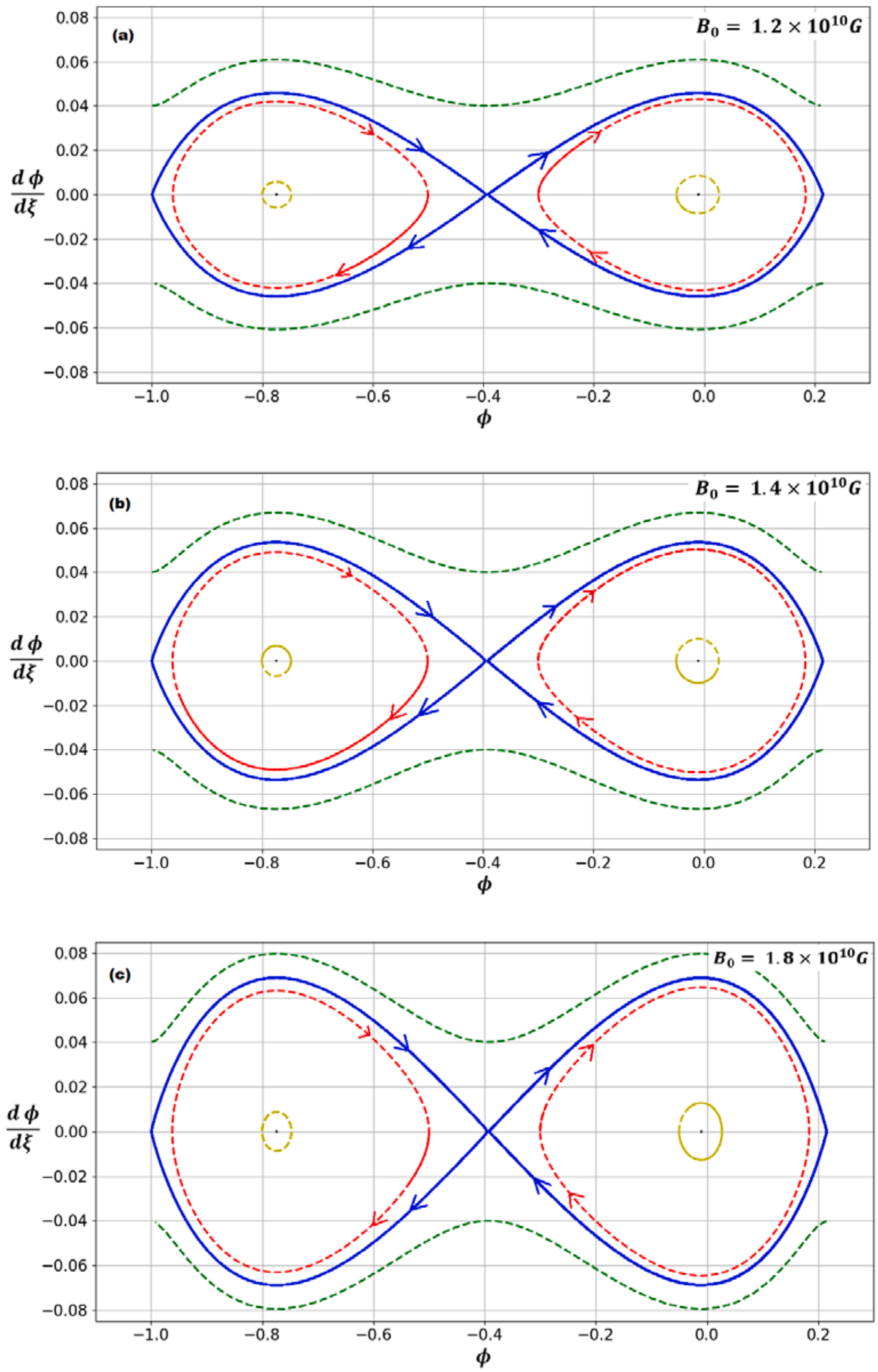

Fig. 5. Phase portrait of the system (16) for different value of $B_0 = 1.2 \times 10^{10}G$, $1.4 \times 10^{10}G$ and $1.8 \times 10^{10}G$. The values of other parameters are $\alpha = 0.1$, $\upsilon_{in} = 3\times\ 10^{13}s^{-1}$, $v_{de} = 0.4$ and $\theta = 60^{\circ}$. Three different phase portraits for different values of B_0 and in these phase portraits the blue solid curve lines are the NHOs correspond to the shock profiles while red and yellow dashed lines are the NPOs. (For interpretation of the references to colour in this figure legend, the reader is referred to the web version of this article.)

$$\frac{\partial^2}{\partial t^2}(1+\phi)^{3/2} - \alpha\frac{\partial^2}{\partial t^2}\left(1-\frac{\phi}{\alpha^{\frac{2}{3}}}\right)^{\frac{3}{2}} - (1-\alpha)\frac{\upsilon_{in}}{\omega_{ci}}\frac{\partial}{\partial t}\frac{\partial^2\phi}{\partial y^2} + \frac{3}{2}v_{de}(1-\alpha)\frac{\partial^2\phi}{\partial t\partial y} - (1-\alpha)\frac{\partial^2\phi}{\partial z^2} = 0. \quad (8)$$

In obtaining Eq. (8), we have used the normalizations $t = \omega_{ci}t, y = \frac{y}{\rho_i}$ and $z = \frac{z}{\rho_i}$. Here, $v_{de} = -\frac{2}{3}\frac{c\varepsilon_{Fe}}{eB_0}\frac{1}{c_s n_{e0}}\frac{\partial n_{e0}}{\partial x}$, $v_{dp} = \frac{2}{3}\frac{c\varepsilon_{Fp}}{eB_0}\frac{1}{c_s n_{p0}}\frac{\partial n_{p0}}{\partial x}$ are normalized (by the ion sound velocity) fluid drift velocities for the electrons and positrons, respectively and α is the ratio of number densities of positrons and electrons at equilibrium, i.e. $\alpha = \frac{n_{p0}}{n_{e0}}$, $c_s = \sqrt{\frac{\varepsilon_{Fe}}{m_i}}$ is the quantum ion acoustic speed and $\rho_i = \frac{c_s}{\omega_{ci}}$ is ion Larmor radius. Equation (8) is the nonlinear evolution equation for drift ion acoustic waves and the effect of adiabatic trapping on the nonlinearity (due to the quantum nature of the electrons and positrons) appears through the terms $(1+\phi)^{3/2}$ and $(1-\frac{\phi}{\alpha^{2/3}})^{\frac{3}{2}}$, respectively.

Before we go on to consider fully nonlinear Eq. (8), we investigate the linear properties of the *epi* plasma by deriving the linear dispersion relation for the drift ion acoustic wave. To this end, we linearize Eq. (8) using a plane wave solution, i.e. $exp\{\imath(k_y y + k_z z - \omega t)\}$ (where, k_y and k_z are the wave numbers perpendicular and parallel to the external magnetic field, respectively and ω is the wave frequency) and obtain the following linear dispersion relation for drift ion acoustic waves in an *epi*

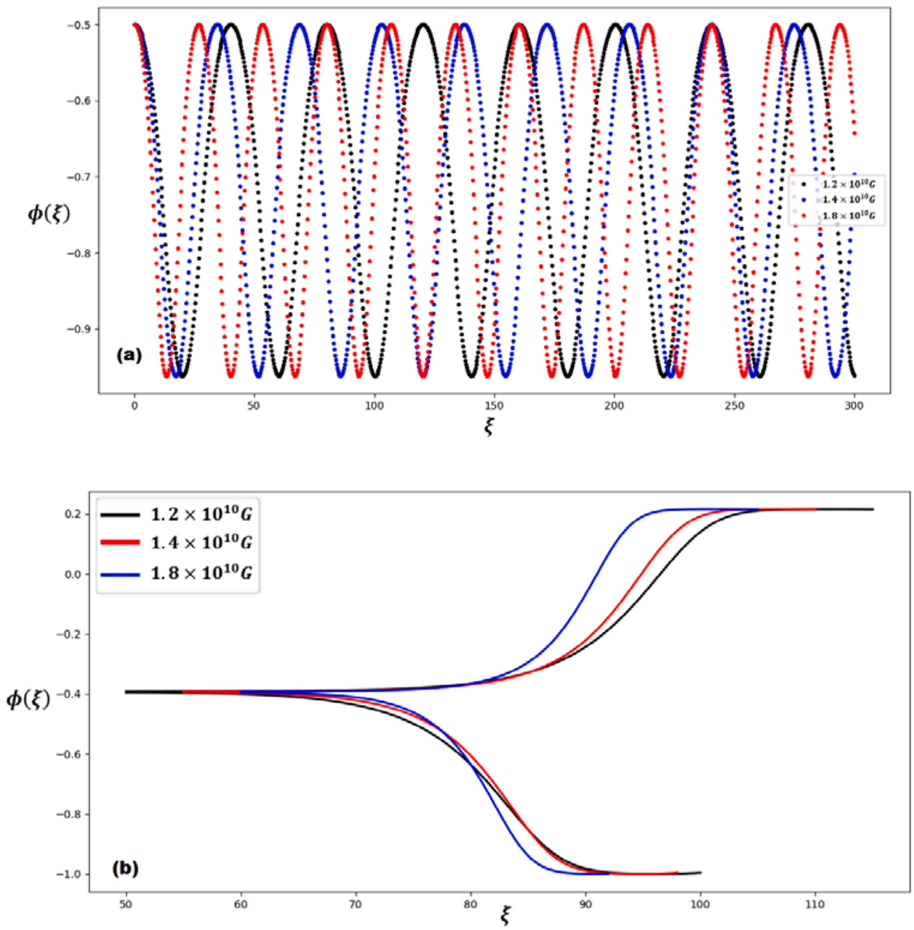

Fig. 6. The time series plots (Fig. 6(a)) and the pair of shock profiles (Fig. 6(b)) of the system (16) for different value of $B_0 = 1.2\times10^{10}G$, $1.4\times10^{10}G$ and $1.8\times10^{10}G$. The values of other parameters are $\alpha = 0.1, \upsilon_{in} = 3\times10^{13}s^{-1}$, $v_{de} = 0.4$ and $\theta = 60^{\circ}$. The time series plots correspond to the red dashed line of NPO_2 in Fig. 5 while the pair of shock profiles correspond to the blue solid line of NHO_1 and HNO_2 in Fig. 5. (For interpretation of the references to colour in this figure legend, the reader is referred to the web version of this article.)

plasma.

$$\frac{3}{2}\left(1-\alpha^{\frac{1}{3}}\right)\omega^2+(1-\alpha)k_y\left(\iota\frac{\upsilon_{in}}{\omega_{ci}}k_y+\frac{3}{2}v_{de}\right)\omega-(1-\alpha)k_z^{\,2}=0. \tag{9}$$

We note here that in our earlier paper-1, where an electron ion plasma was considered, we had obtained a nonlinear evolution equation similar to Eq. (8) but without positrons and showed that the equation was fully integrable and had a form structurally similar to Burgers equation and obtained shock solutions. However, in the present case, due to the presence of positrons, our nonlinear equation (Eq. (8)) is not fully integrable and thus we resort to a dynamical analysis, which we take up in the next section.

Dynamical system of coupled drift acoustic shock wave in *epi* plasma and phase portrait analysis

In this section, we will modify the nonlinear evolution Eq. (8) to express it in the form of coupled nonlinear dynamical equations. For this, we shift to a comoving frame of reference defined as follows.

$$\xi=\eta_y y+\eta_z z-vt, \tag{10}$$

where η_y and η_z are the directional cosines along the y-axis and z-axis, respectively, and v is the velocity of the nonlinear structure. The modified form of the Eq. (8) reads.

$$v^2\frac{d^2}{d\xi^2}(1+\phi)^{3/2}-\alpha v^2\frac{d^2}{d\xi^2}\left(1-\alpha^{-\frac{2}{3}}\phi\right)^{\frac{3}{2}}+Av\frac{d^3\phi}{d\xi^3}-(Bv+C)\frac{d^2\phi}{d\xi^2}=0, \tag{11}$$

Here, $A=\eta_y^2(1-\alpha)\frac{\upsilon_{in}}{\omega_{ci}}$, $B=\frac{3}{2}\eta_y v_{de}(1-\alpha)$ and $C=(1-\alpha)\eta_z^2$. Integrating Eq. (11) twice, we obtain

$$v^2(1+\phi)^{3/2}-\alpha v^2\left(1-\alpha^{-\frac{2}{3}}\phi\right)^{\frac{3}{2}}+Av\frac{d\phi}{d\xi}-(Bv+C)\phi+c_2=0, \tag{12}$$

In obtaining the above equation, we have used the boundary conditions, i.e., when $\xi\to\pm\infty$ then $\phi\to\phi_{R,L}$ as considered in paper-1. The first constant of integration c_1 becomes zero while the second constant of integration c_2 is evaluated after applying the above-mentioned boundary conditions and is given below.

$$v^2(1+\phi_R)^{3/2}-\alpha v^2\left(1-\alpha^{-\frac{2}{3}}\phi_R\right)^{\frac{3}{2}}-(Bv+C)\phi_R=c_2, \tag{13}$$

$$v^2(1+\phi_L)^{3/2}-\alpha v^2\left(1-\alpha^{-\frac{2}{3}}\phi_L\right)^{\frac{3}{2}}-(Bv+C)\phi_L=c_2. \tag{14}$$

The value of normalized ϕ ranges from -1 to $\alpha^{\frac{2}{3}}$, where $\alpha^{\frac{2}{3}}$ ensures that the term remains real. We obtain an expression of the velocity v of the shock propagation by solving Eqs. (13) and (14) which reads as.

$$v=\frac{B\phi_A\pm\sqrt{B^2\phi_A+4C\phi_A\left(\phi_C+\phi_L\phi_C-\alpha\phi_D+\alpha^{\frac{1}{3}}\phi_D-\phi_B-\phi_B\phi_R+\alpha\phi_E-\alpha^{\frac{1}{3}}\phi_R\phi_E\right)}}{2\left(\phi_C+\phi_L\phi_C-\alpha\phi_D+\alpha^{\frac{1}{3}}\phi_L\phi_D-\phi_B-\phi_B\phi_R+\alpha\phi_E-\alpha^{\frac{1}{3}}\phi_R\phi_E\right)}, \tag{15}$$

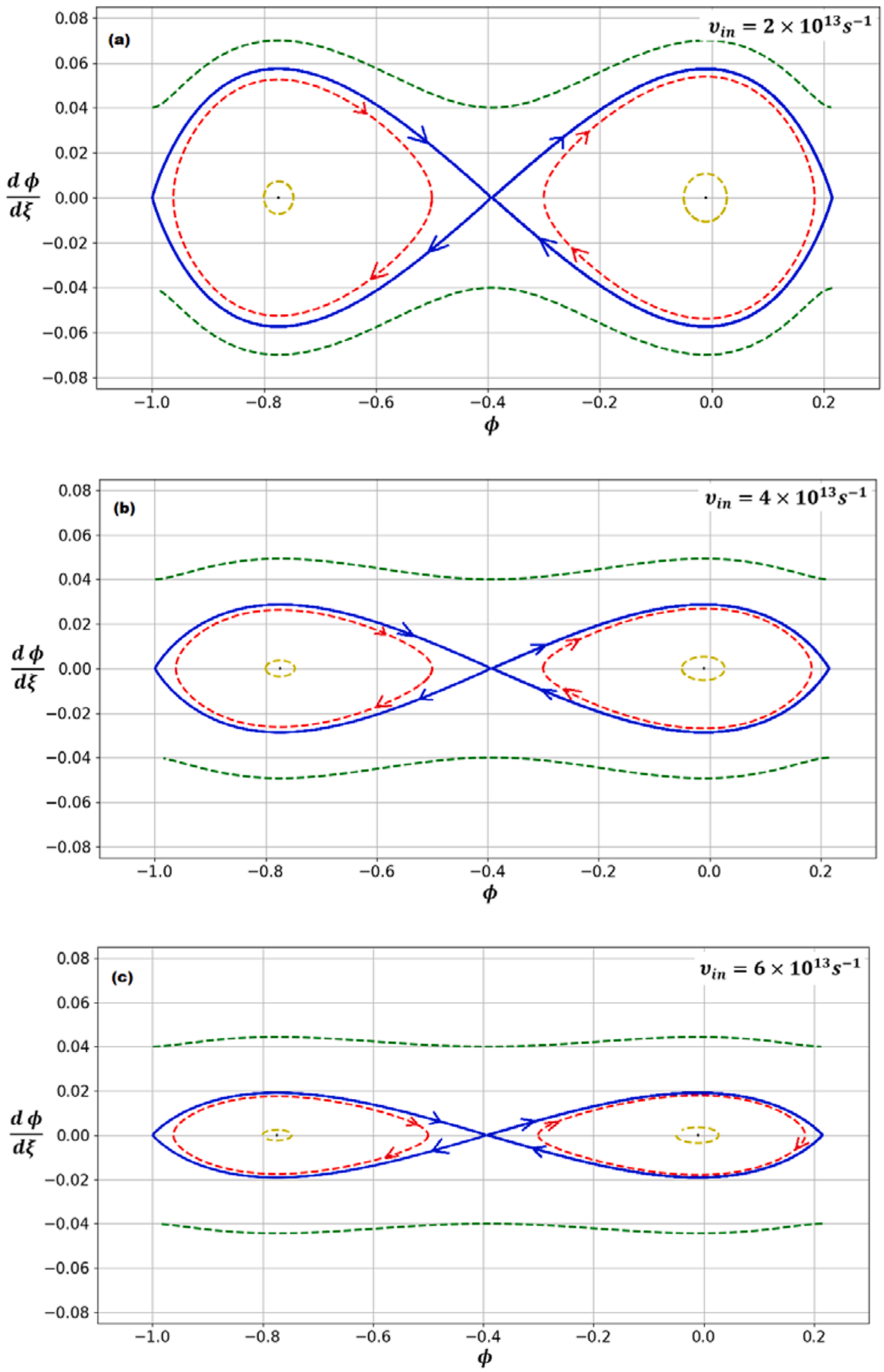

Fig. 7. Phase portrait of the system (16) for different value of collisional frequency, $\upsilon_{in} = 2 \times 10^{13} s^{-1}$, $4 \times 10^{13} s^{-1}$ and $6 \times 10^{13} s^{-1}$. The values of other parameters are $\alpha = 0.1, B_0 = 10^{10} G, \nu_{de} = 0.4$ and $\theta = 60^{\circ}$. Three different phase portraits for different values of υ_{in} and in these phase portraits the blue solid curve lines are the NHOs correspond to the pair of shock profiles while red and yellow dashed lines are the NPOs. (For interpretation of the references to colour in this figure legend, the reader is referred to the web version of this article.)

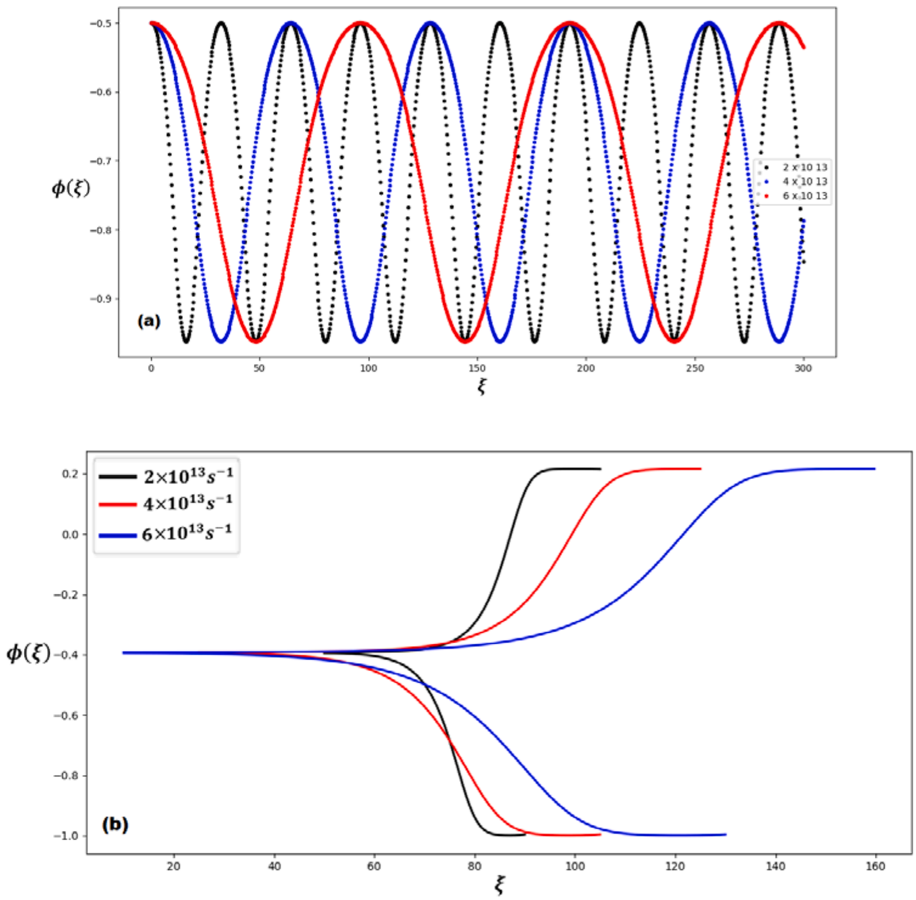

Fig. 8. Time series plots (Fig. 8(a)) and shock profiles (Fig. 8(b)) of the system (16) for different value of collisional frequency $\upsilon_{in} = 2\times10^{13}s^{-1}$, $4\times10^{13}s^{-1}$ and $6\times10^{13}s^{-1}$. The values of other parameters are $\alpha = 0.1, B_0 = 10^{10}G, \nu_{de} = 0.4$ and $\theta = 60^{\circ}$. The time series plots corresponds to the red dashed line of NPO_2 in Fig. 7 while the pair of shock profiles correspond to the blue solid line of NHO_1 and HNO_2 in Fig. 7. (For interpretation of the references to colour in this figure legend, the reader is referred to the web version of this article.)

Here, $\phi_A = (\phi_L - \phi_R)$, $\phi_B = \sqrt{1+\phi_L}$, $\phi_C = \sqrt{1+\phi_R}$, $\phi_D = \sqrt{1-\frac{\phi_L}{\alpha^{\frac{2}{3}}}}$, and $\phi_E = \sqrt{1-\frac{\phi_R}{\alpha^{\frac{2}{3}}}}$.

Unlike the expression obtained for the *ei* plasma in paper-1, Eq. (12) cannot be integrated and, therefore, to proceed further, we transform the equation into a pair of first order nonlinear autonomous equations by following the work of Saha *et al.* [40].

$$\frac{d\phi}{d\xi} = y$$
$$\frac{dy}{d\xi} = \frac{1}{(A\ v)^2}\left[-\frac{3}{2}v^2(1+\phi)^{\frac{1}{2}} - \frac{3}{2}\alpha^{\frac{1}{3}}v^2\left(1-\alpha^{-\frac{2}{3}}\phi\right)^{\frac{1}{2}} + Bv + C\right] \left[-v^2(1+\phi)^{\frac{3}{2}} + \alpha v^2\left(1-\alpha^{-\frac{2}{3}}\phi\right)^{\frac{3}{2}} + (Bv+C)\phi + c_2\right], \tag{16}$$

We note the Hamiltonian of this system is given by

$$H = \frac{y^2}{2} - \frac{1}{2(Av)^2}\Bigg[-2c_2(1+\phi)^{\frac{3}{2}}v^2 - 2(1+\phi)^{\frac{5}{2}}v^2(Bv+C) + (1+\phi)^2\left(C^2+2BCv+B^2v^2+3\left(1+\alpha^{\frac{2}{3}}\right)v^4\right) + (1+\phi)\left(2Cc_2+2Bc_2v-3\left(1+\alpha^{\frac{2}{3}}\right)^2v^4\right) + 2\alpha^{\frac{1}{3}}\left(1-\alpha^{-\frac{2}{3}}\phi\right)^{\frac{1}{2}}v^2\Big\{\left(1+\alpha^{\frac{2}{3}}\right)c_2 - \left(1+\alpha^{\frac{2}{3}}\right)(1+\phi)^{\frac{3}{2}}v^2 + (1+\phi)^{\frac{5}{2}}v^2 - (1+\phi)^2(Bv+C) + (1+\phi)\left(\left(1+\alpha^{\frac{2}{3}}\right)C - c_2 + \left(1+\alpha^{\frac{2}{3}}\right)Bv\right)\Big\}\Bigg]. \tag{17}$$

Eq. (16) is a planar dynamical system with physical parameters α, B_0, υ_{in}, υ_{de} and θ and to examine the dynamics of this nonlinear system, we employ the phase portrait analysis of the dynamical system equation (16).

Phase portrait and time series analysis dependence on various physical parameters

For this analysis, we have chosen the following parameter values $\alpha = 0.1$, $\upsilon_{in} = 3\times10^{13}s^{-1}$, $B_0 = 10^{10}G$, $\nu_{de} = 0.4$, $\theta = 60^{\circ}$. We can see in Fig. 1 that there are five fixed points $F_0(\phi_0, 0)$, $F_1(\phi_1, 0)$, $F_2(\phi_2, 0)$, $F_3(\phi_3, 0)$ and $F_4(\phi_4, 0)$. Here, $F_1(\phi_1, 0)$ and $F_3(\phi_3, 0)$ are the two centers, while $F_0(\phi_0, 0)$, $F_1(\phi_1, 0)$ and $F_4(\phi_4, 0)$ can be shown to be saddle points. We note that these fixed points are found numerically. Note that initially, we carry out this analysis for the positive root of ν (upper sign in the expression (15)). We further determine the nonlinear heteroclinic orbits (NHOs) around the centers $F_1(\phi_1, 0)$ and $F_3(\phi_3, 0)$ and see these two orbits i.e., NHO_1 and NHO_2. We see that in Fig. 1, there are two types of qualitatively different nonlinear orbits. In the first type of nonlinear orbit, there are two pairs of NHOs and, in the second type, there are two families of nonlinear periodic orbits (NPOs). NHO_1 is the first type which is formed by joining the points F_0 with F_2 and F_2 with F_0, whereas NHO_2, the second type, is formed by joining the points F_4 with F_2 and F_2 with F_4. For these two pairs of NHOs represented by solid blue curves, we have a pair of shock structures that, to the best of our knowledge, is reported for the first time. Similarly, for the two families of NPOs, represented by red and yellow dashed lines, we have two families of nonlinear periodic wave orbits around the centers $F_1(\phi_1, 0)$ and $F_3(\phi_3, 0)$. The corresponding periodic wave solutions of red and yellow curves of NPO_1 are shown in Fig. 2. (It is noted here that in the absence of positrons only one NHO is obtained which corresponds to one shock structure and this is discussed as a limiting case at the end of this section). We have presented a time series analysis of Eq. (16) for

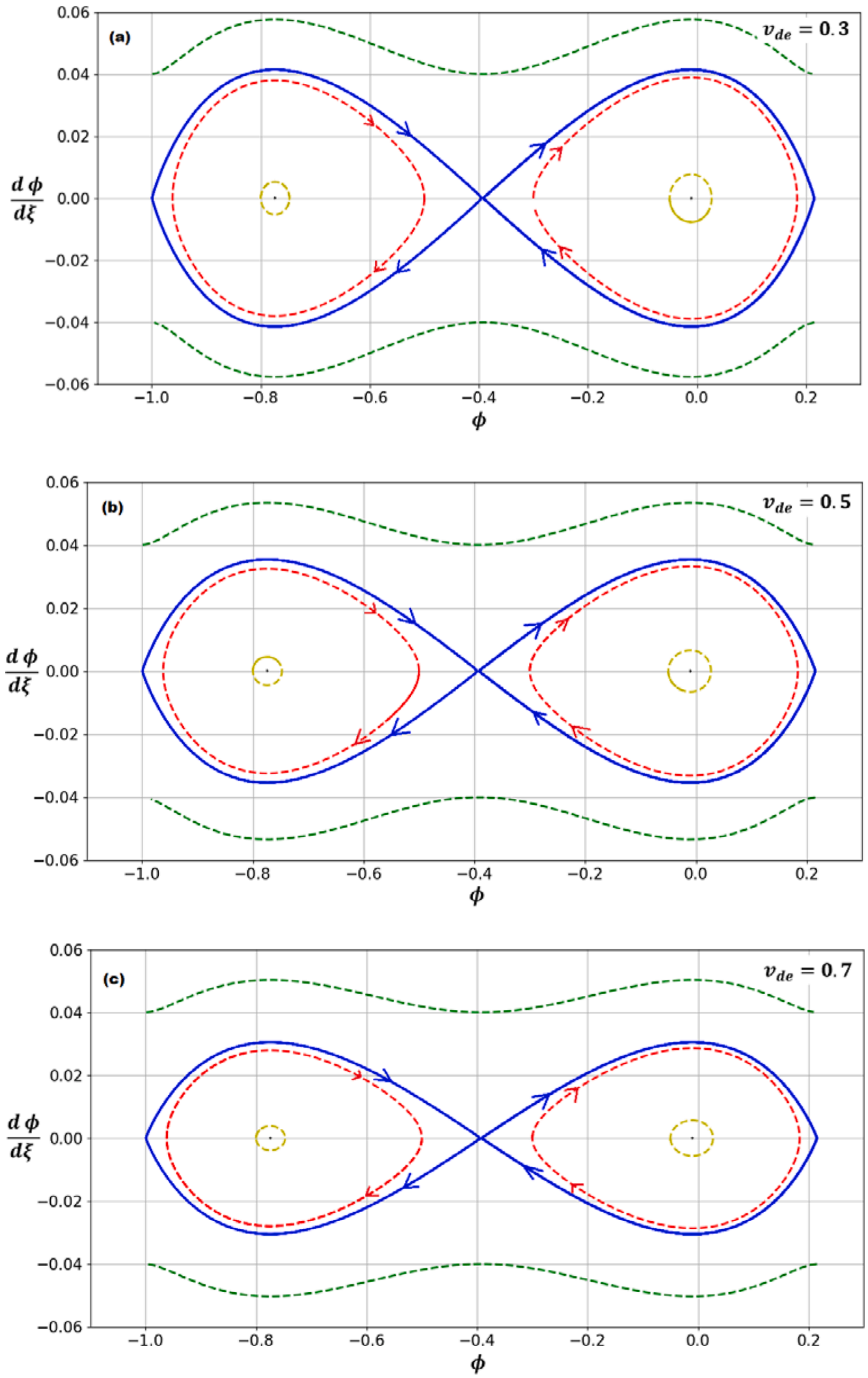

Fig. 9. Phase portrait of the system (16) for different value of $v_{de} = 0.3, 0.5$ and 0.7. The values of other physical parameters are $\alpha = 0.1, B_0 = 10^{10} G, \upsilon_{in} = 3 \times 10^{13} s^{-1}$ and $\theta = 60^{\circ}$. Three different phase portraits for different values of v_{de} and in these phase portraits the blue solid curve lines are the NHOs correspond to the shock profiles while red and yellow dashed lines are the NPOs. (For interpretation of the references to colour in this figure legend, the reader is referred to the web version of this article.)

different periodic orbits as shown in Fig. 1.

The influence of different physical parameters like the ratio of number densities of positrons to electrons α, collisional frequency υ_{in}, magnetic field B_0, drift velocity v_{de} and angle of propagation θ on drift ion acoustic waves in the presence of adiabatic trapping in a quantum *epi* magnetoplasma is investigated. In Fig. 3(a), (b) and (c), we present the phase portraits of the dynamical system Eq. (16) for different values of the positron concentration α. We note that fixed points are different for different values of α and as α decreases, the fixed points move closer to one another. In Fig. 4, we present the time series of $\phi(\xi)$ for different values of α. In Fig. 4a, we show the time series of the periodic orbits and in Fig. 4(b), we obtain the corresponding shock structures (i.e. the time series of the NHOs). The results shown in Fig. 4(b) clearly show pairs of shocks for different values of α, and we see that for a larger concentration of positrons the steepness of the shock structures increases.

Magnetic field B_0 and the collisional frequency υ_{in} are the two other important parameters which affect the *epi* nonlinear wave structures. In Fig. 5, we present the phase portraits, time series plots and shock profiles for different values of B_0. We see from Fig. 5a, b and c that by increasing the value of B_0, the distance between the center points increases. In Fig. 6, we show the corresponding (to Fig. 5) time series of the periodic orbits and shock profiles respectively. In Fig. 7, the phase portraits are

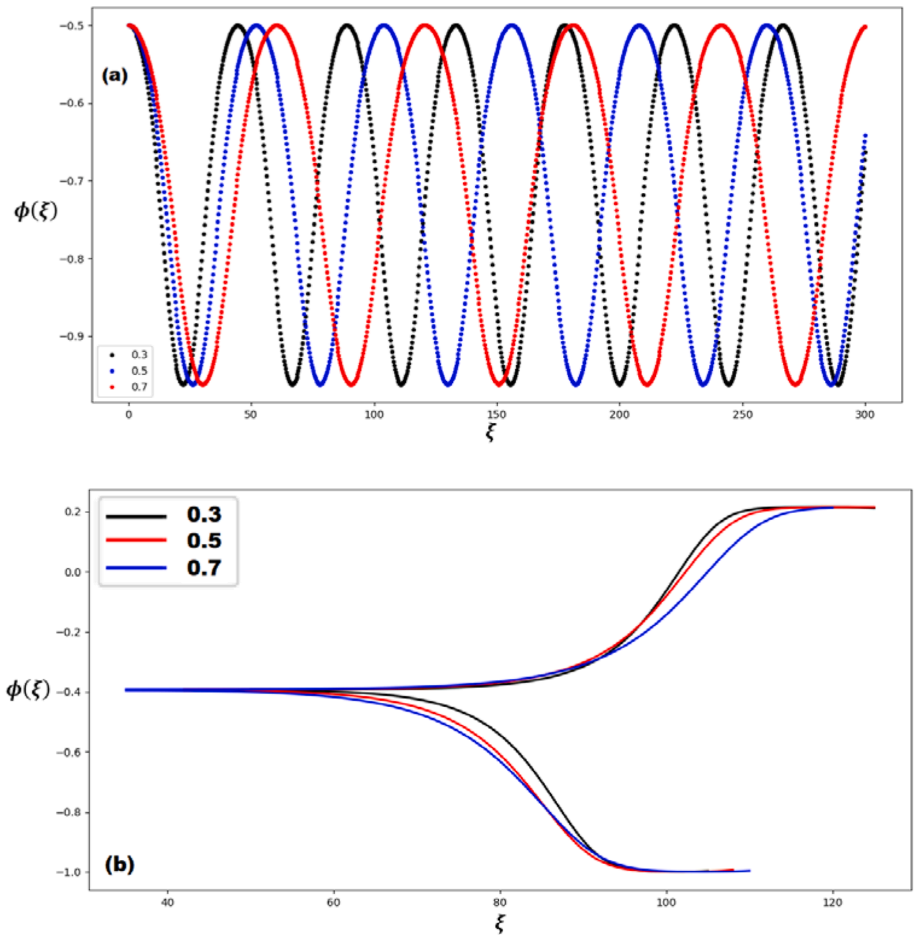

Fig. 10. Time series plots (Fig. 10(a)) and the pair of shock profiles (Fig. 10(b)) of the system (20) for different value of $v_{de} = 0.3, 0.5$ and 0.7. The values of other physical parameters are $\alpha = 0.1$, $B_0 = 10^{10}G$, $\upsilon_{in} = 3\times 10^{13}s^{-1}$ and $\theta = 60^{\circ}$. The time series plots correspond to the red dashed line of NPO_2 in Fig. 9 while the pair of shock profiles correspond to the blue solid line of NHO_1 and HNO_2 in Fig. 9. (For interpretation of the references to colour in this figure legend, the reader is referred to the web version of this article.)

shown for the variation of the collision frequency keeping the other parameters fixed. We see from Fig. 7a, b and c that the distance between the center points $F_1(\phi_1, 0)$ and $F_3(\phi_3, 0)$ decreases by increasing the value of υ_{in}, however, the positions of the fixed points remain the same in both cases. In Fig. 8(a), we show the corresponding (Fig. 7) time series evolution of periodic orbits, and it is observed that the wavelength increases. The shock profiles, shown in Fig. 8(b), manifest that by increasing the value of υ_{in}, the steepness of the shock profile decreases. Fig. 8(a) indicates that the wavelength of the periodic wave increases by increasing the value of υ_{in}. Furthermore, the steepness of the shock profile decreases by increasing the value of collision frequency υ_{in} (see Fig. 8(b)).

Furthermore, two other parameters which modify the solutions of nonlinear periodic waves are the inhomogeneity v_{de} and angle of propagation θ. We vary the value of v_{de} from 0.3 to 0.7 (see Figs. 9 and 10) and θ from 60° to 70° (see Figs. 11 and 12). In Figs. 9 and 11, we find that by increasing the values of v_{de} and, the distance between the center points $F_1(\phi_1, 0)$ and $F_3(\phi_3, 0)$ increases and the distances between the invariant points remain the same. In the case of θ, the increase in distance between the centre points is very small. It is also observed that by increasing the value of v_{de} and θ, the wavelength of the nonlinear periodic waves decreases (see Fig. 10(a) and Fig. 12(a)). According to Fig. 10 (b) and Fig. 12(b), the steepness of the shock profiles increases by increasing the value of v_{de} and θ. In Fig. 11, we note that small variations take place in the phase portraits by varying the angle of propagation as can be seen in time series plots in Fig. 12(a).

In Fig. 13, we carry out the phase space analysis for the negative root of v (Eq. (15)) and we observe behavior similar to the positive sign, however, the numerical values are different. To avoid repetition, the figures are not shown here.

Limiting case: Here for the sake of completeness, we present the phase portrait analysis in the absence of positrons i.e. extending the results of our earlier paper-1 to nonlinear dynamical analysis. In this case, Eq. (16) reduces to.

$$\frac{d\phi}{d\xi} = y$$
$$\frac{dy}{d\xi} = \frac{1}{(A\ v)^2}\left[-\frac{3}{2}v^2(1+\phi)^{\frac{1}{2}} + Bv + C\right] \left[-v^2(1+\phi)^{\frac{3}{2}} + (Bv+C)\phi + c_2\right], \tag{18}$$

and the coefficients A, B and C reduce to, $A = \eta_y^2 \frac{\upsilon_{in}}{\omega_{ci}}$, $B = \frac{3}{2}\eta_y v_{de}$ and $C = \eta_z^2$. The corresponding expressions of v and c_2 reduce, respectively to.

$$v = \frac{B\phi_A \pm \sqrt{B^2\phi_A + 4C\phi_A\{\phi_C + \phi_L\phi_C - \phi_B - \phi_B\phi_R\}}}{2(\phi_C + \phi_L\phi_C - \phi_B - \phi_B\phi_R)}, \tag{19}$$

where $\phi_A = (\phi_L - \phi_R)$, $\phi_B = \sqrt{1+\phi_L}$, $\phi_C = \sqrt{1+\phi_R}$ and

$$v^2(1+\phi_R)^{3/2} - (Bv+C)\phi_R = c_2,$$

$$v^2(1+\phi_L)^{3/2} - (Bv+C)\phi_L = c_2. \tag{20}$$

Fig. 14 shows the results of our phase space analysis of Eq. (18) (along with the expressions (19) and (20)) and we see that, as expected, only one shock structure is obtained.

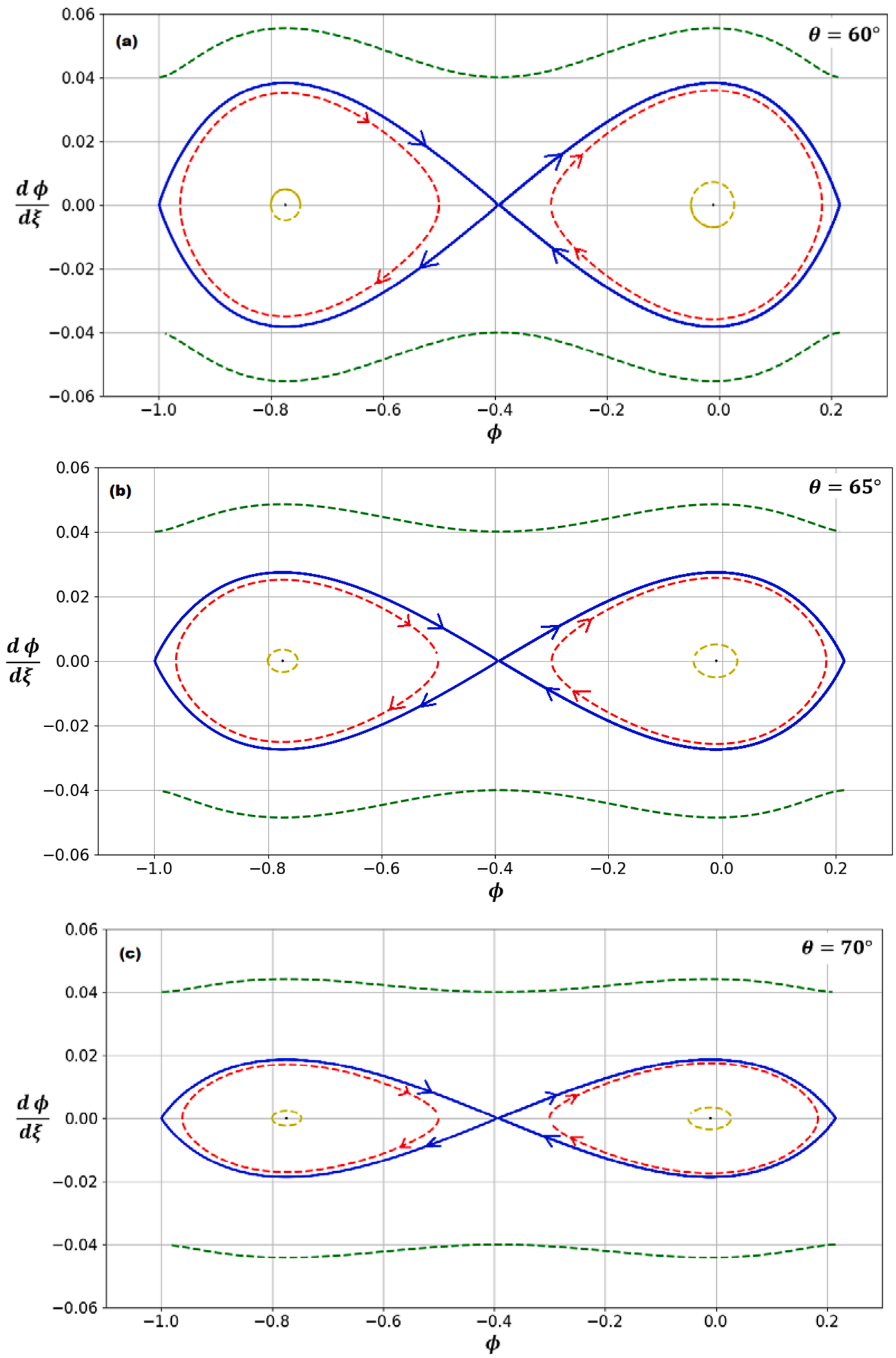

Fig. 11. Phase portrait of the system (16) for different values of $\theta = 60^{\circ}, 65^{\circ}$ and 70°. The values of other parameters are $\alpha = 0.1$, $B_0 = 10^{10}G$, $v_{de} = 0.4$and $\nu_{in} = 3\times 10^{13}s^{-1}$. Three different phase portraits for different values of θ and in these phase portraits the blue solid curve lines are the NHOs correspond to the shock profiles while red and yellow dashed lines are the NPOs. (For interpretation of the references to colour in this figure legend, the reader is referred to the web version of this article.)

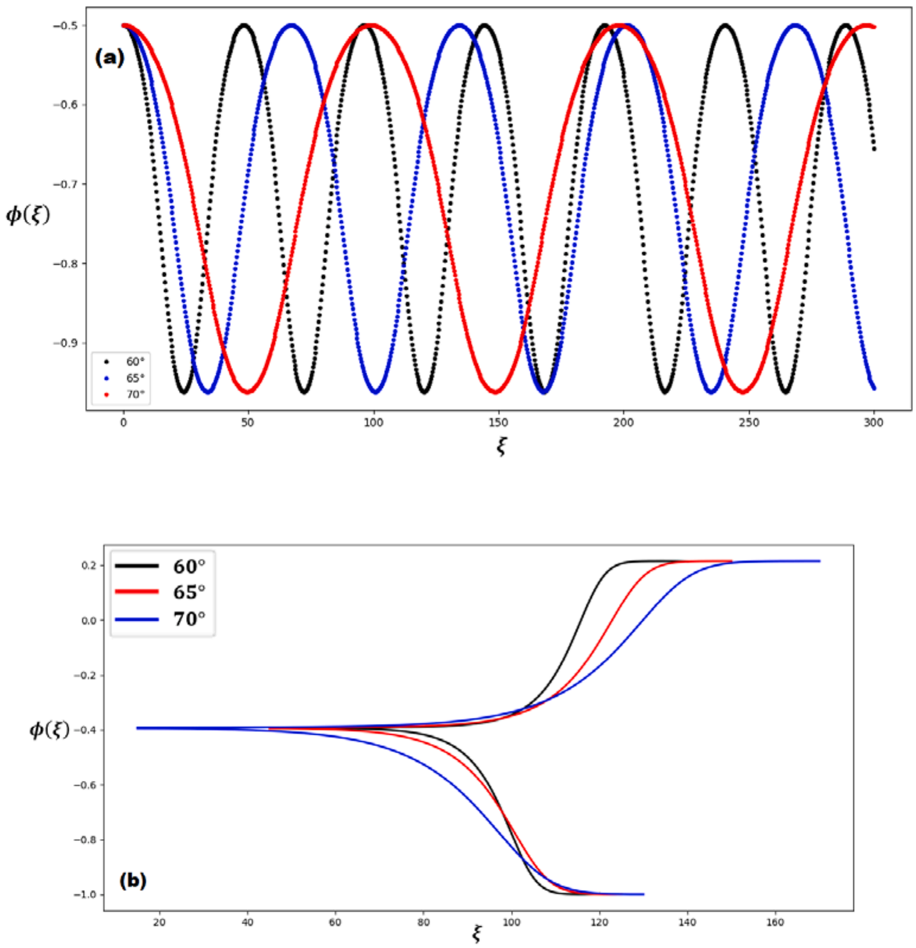

Fig. 12. Time series plots (Fig. 12(a)) and the pair of shock profiles (Fig. 12(b)) of the system (16) for different value of $\theta = 60^{\circ}, 65^{\circ}$ and 70°. The values of other parameters are $\alpha = 0.1$, $B_0 = 10^{10}G$, $v_{de} = 0.4$ and $v_{in} = 3 \times 10^{13}s^{-1}$. The time series plots correspond to the red dashed line of NPO_2 in Fig. 11 while the pair of shock profiles correspond to the blue solid line of NHO_1 and HNO_2 in Fig. 11. (For interpretation of the references to colour in this figure legend, the reader is referred to the web version of this article.)

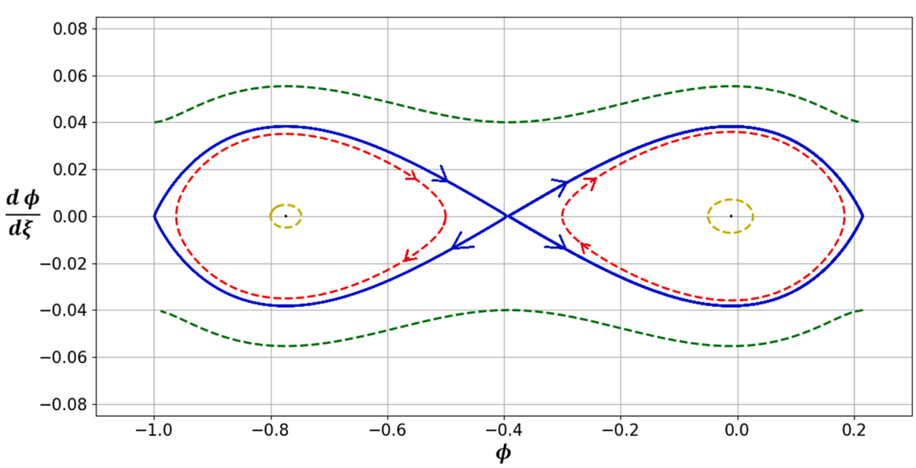

Fig. 13. Phase portrait of the system (16) with negative root of the velocity v for $\alpha = 0.1$, $v_{in} = 3 \times 10^{13}s^{-1}$, $B_0 = 10^{10}G$, $v_{de} = 0.4$ and $\theta = 60^{\circ}$. The blue solid curve lines are the NHOs correspond to the shock profile while red and yellow dashed lines are the NPOs. $F_0(\phi_0, 0)$, $F_1(\phi_1, 0)$, $F_2(\phi_2, 0)$, $F_3(\phi_3, 0)$ and $F_4(\phi_4, 0)$ are the fixed points of the nonlinear dynamical system (16). (For interpretation of the references to colour in this figure legend, the reader is referred to the web version of this article.)

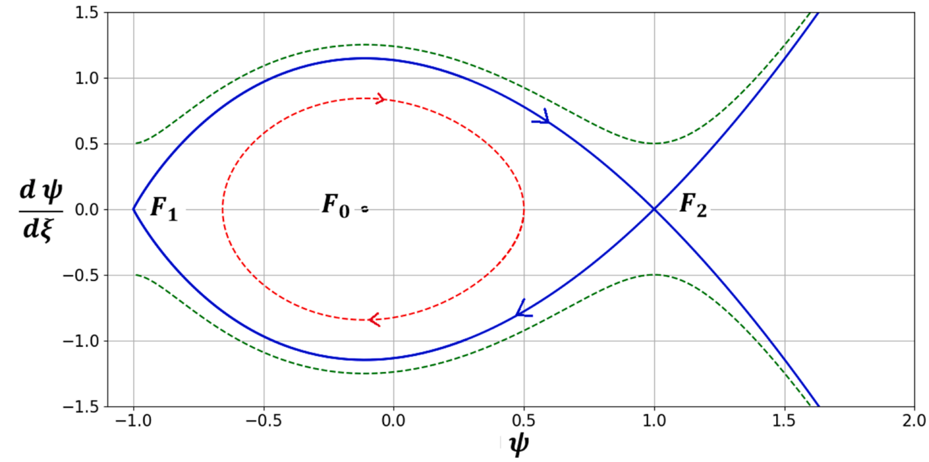

Fig. 14. Phase portrait of the system (14) for $n_0 = 10^{27} cm^{-1}$, $\upsilon_{in} = 3 \times 10^{13} s^{-1}$, $B_0 = 10^{10} G$, $v_{de} = 0.4$ and $\theta = 60^{\circ}$. The blue solid lines correspond to the shock profile plotted in paper 1. (For interpretation of the references to colour in this figure legend, the reader is referred to the web version of this article.)

Summary and conclusion

In this work, we have investigated ion acoustic shock waves in fully degenerate quantum *epi* plasmas in the presence of adiabatically trapped electrons. Using the QMHD model, we have derived a novel equation that contains terms with fractional nonlinearities. Complex nonlinearities make it difficult to find the solution to this equation using the analytical approach and, therefore, phase plane theory has been used to solve the system under consideration. To justify our *epi* plasma results, the dynamical system of *ei* plasma [48] is also solved by using phase plane theory. The most significant finding of this work is the formation of a pair of shock structures which is reported for the first time in literature to the best of our knowledge. Furthermore, the effect of different controlling parameters such as the ratio of number of positrons and electrons α, collisional frequency υ_{in}, magnetic field B_0, drift velocity v_{de} and angle of propagation θ on phase portraits, time series plots and shock profiles have also been explored.

Declaration of Competing Interest

The authors declare that they have no known competing financial interests or personal relationships that could have appeared to influence the work reported in this paper.

Data availability

No data was used for the research described in the article.

Acknowledgement

This research was supported by the Higher Education Commission (HEC), Pakistan Project No. 7558/Punjab/NRPU/R&D/HEC/2017. One of the authors W. Masood acknowledges support from the Abdus Salam International Centre for Theoretical Physics (AS-ICTP) for his visit under the Regular Associateship Scheme.

References

[1] Misner CW. K, S. Thorne, JA Wheeler, Gravitation, vol. 1. WH Freeman Company, San Francisco; 1973.
[2] Rees M, Gibbons G, Hawking S, Siklas S. The very early universe. Cambridge: Cambridge University Press; 1983.
[3] Dubinov A, Kolotkov DY, Sazonkin M. Nonlinear theory of ion-sound waves in a dusty electron-positron-ion plasma. Tech Phys 2012;57(5):585–93.
[4] Cheng L-H, Tang R-A, Zhang A-X, Xue J-K. Nonlinear interaction of intense laser pulses and an inhomogeneous electron-positron-ion plasma. Phys Rev E 2013;87 (2):025101.
[5] Miller H, Witta P. Active Galactic Nuclei Springer-Verlag. Berlin; 1987.
[6] Tandberg-Hanssen E, Emslie AG. The physics of solar flares. Cambridge University Press; 1988.
[7] Goldreich P, Julian WH. Pulsar electrodynamics. Astrophys J 1969;157:869.
[8] Michel FC. Theory of pulsar magnetospheres. Rev Mod Phys 1982;54(1):1.
[9] Surko C, Leventhal M, Crane W, Passner A, Wysocki F, Murphy T, et al. Use of positrons to study transport in tokamak plasmas. Rev Sci Instrum 1986;57(8): 1862–7.
[10] Tinkle M, Greaves R, Surko C, Spencer R, Mason G. Low-order modes as diagnostics of spheroidal non-neutral plasmas. Phys Rev Lett 1994;72(3):352.
[11] Greaves R, Surko C. An electron-positron beam-plasma experiment. Phys Rev Lett 1995;75(21):3846.
[12] El-Bedwehy N, Moslem W. Zakharov-Kuznetsov-Burgers equation in superthermal electron-positron-ion plasma. Astrophys Space Sci 2011;335(2):435–42.
[13] Iqbal M, Masood W, Shah HA, Tsintsadze N. Nonlinear density excitations in electron-positron-ion plasmas with trapping in a quantizing magnetic field. Phys Plasmas 2017;24(1):014503.
[14] Manfredi G. How to model quantum plasmas. Fields Inst Commun 2005;46: 263–87.
[15] Jahan S, Sharmin BE, Chowdhury NA, Mannan A, Roy TS, Mamun A. Electrostatic ion-acoustic shock waves in a magnetized degenerate quantum plasma. Plasma 2021;4:426–34.
[16] Mamun A, Sharmin B, Tamanna N. Roles of degenerate quantum plasma temperature and stationary heavy nucleus species in nucleus-acoustic shock waves. Results Phys 2021;29:104799.
[17] Mamun A, Amina M, Schlickeiser R. Nucleus-acoustic shock structures in a strongly coupled self-gravitating degenerate quantum plasma. Phys Plasmas 2016;23: 094503.
[18] Markowich PA, Ringhofer CA, Schmeiser C. Semiconductor equations. Springer Science & Business Media; 2012.
[19] Ang L, Kwan T, Lau Y. New scaling of Child-Langmuir law in the quantum regime. Phys Rev Lett 2003;91:208303.
[20] Killian TC. Cool vibes. Nature 2006;441:297–8.
[21] Jung Y-D. Quantum-mechanical effects on electron–electron scattering in dense high-temperature plasmas. Phys Plasmas 2001;8:3842–4.
[22] Khan S, Masood W. Linear and nonlinear quantum ion-acoustic waves in dense magnetized electron-positron-ion plasmas. Phys Plasmas 2008;15(6):062301.
[23] Masood W, Jehan N, Mirza AM, Sakanaka P. Planar and non-planar ion acoustic shock waves in electron–positron–ion plasmas. Phys Lett A 2008;372(23):4279–82.
[24] Mamun A. Cylindrical and spherical nucleus-acoustic solitary and shock waves in degenerate electron-nucleus plasmas. Physics 2021;3:1088–97.
[25] Mamun A, Akter J. Degenerate pressure driven self-gravito-acoustic solitary and shock structures. Results Phys 2022;32:105072.
[26] Nejoh Y. The effect of the ion temperature on large amplitude ion-acoustic waves in an electron–positron–ion plasma. Phys Plasmas 1996;3(4):1447–51.
[27] Verheest F, Cattaert T. Large amplitude solitary electromagnetic waves in electron-positron plasmas. Phys Plasmas 2004;11(6):3078–82.
[28] Banerjee G, Dutta S, Misra A. Large amplitude electromagnetic solitons in a fully relativistic magnetized electron-positron-pair plasma. Adv Space Res 2020;66(9): 2265–73.
[29] Rizzato F. Weak nonlinear electromagnetic waves and low-frequency magnetic-field generation in electron-positron-ion plasmas. J Plasma Phys 1988;40(2): 289–98.
[30] Berezhiani V, El-Ashry M, Mofiz U. Theory of strong-electromagnetic-wave propagation in an electron-positron-ion plasma. Phys Rev E 1994;50(1):448.
[31] Ali S, Moslem W, Shukla P, Schlickeiser R. Linear and nonlinear ion-acoustic waves in an unmagnetized electron-positron-ion quantum plasma. Phys Plasmas 2007;14 (8):082307.
[32] Mushtaq A, Khan S. Ion acoustic solitary wave with weakly transverse perturbations in quantum electron-positron-ion plasma. Phys Plasmas 2007;14(5): 052307.

[33] Kumar Samanta U, Saha A, Chatterjee P. Bifurcations of nonlinear ion acoustic travelling waves in the frame of a Zakharov-Kuznetsov equation in magnetized plasma with a kappa distributed electron. Phys Plasmas 2013;20(5):052111.
[34] Samanta UK, Saha A, Chatterjee P. Bifurcations of dust ion acoustic travelling waves in a magnetized quantum dusty plasma. Astrophys Space Sci 2013;347(2):293–8.
[35] Saha A, Chatterjee P. Bifurcations of electron acoustic traveling waves in an unmagnetized quantum plasma with cold and hot electrons. Astrophys Space Sci 2014;349(1):239–44.
[36] Rahim Z, Adnan M, Qamar A, Saha A. Nonplanar dust-acoustic waves and chaotic motions in Thomas Fermi dusty plasmas. Phys Plasmas 2018;25(8):083706.
[37] Islam M, Biswas S, Chowdhury N, Mannan A, Salahuddin M, Mamun A. Obliquely propagating ion-acoustic shock waves in a degenerate quantum plasma. Contrib Plasma Phys 2022;62:e202100073.
[38] Saha A. Nonlinear excitations for the positron acoustic shock waves in dissipative nonextensive electron-positron-ion plasmas. Phys Plasmas 2017;24(3):034502.
[39] El-Monier S, Atteya A. Bifurcation analysis for dust-acoustic waves in a four-component plasma including warm ions. IEEE Trans Plasma Sci 2017;46(4):815–24.
[40] Saha A, Pradhan B, Banerjee S. Bifurcation analysis of quantum ion-acoustic kink, anti-kink and periodic waves of the Burgers equation in a dense quantum plasma. Eur Phys J Plus 2020;135(2):1–13.
[41] Saha A, Banerjee S. Dynamical systems and nonlinear waves in plasmas. CRC Press; 2021.
[42] Bernstein IB, Greene JM, Kruskal MD. Exact nonlinear plasma oscillations. Phys Rev 1957;108(3):546.
[43] Gurevich A. Distribution of captured particles in a potential well in the absence of collisions. Sov Phys JETP 1968;26(3):575–80.
[44] Shah HA, Qureshi MNS, Tsintsadze N. Effect of trapping in degenerate quantum plasmas. Phys Plasmas 2010;17(3):032312.
[45] Shah HA, Masood W, Qureshi MNS, Tsintsadze N. Effects of trapping and finite temperature in a relativistic degenerate plasma. Phys Plasmas 2011;18(10):102306.
[46] Arshad S, Shah HA, Qureshi MNS. Effect of adiabatic trapping on vortices and solitons in degenerate plasma in the presence of a quantizing magnetic field. Phys Scr 2014;89(7):075602.
[47] Fayyaz A, Shah HA, Qureshi MNS, Masood W. Nonlinear drift ion acoustic waves in degenerate plasmas with adiabatic trapping. Phys Scr 2020;95(4):045609.
[48] Fayyaz A, Shah HA, Qureshi MNS, Masood W. Coupled drift ion acoustic shock waves with trapped electrons in quantum magnetoplasma. Phys Scr 2020;95(8):085602.
[49] Tsintsadze N, Shah HA, Qureshi MNS, Tagviashvili M. Properties of solitary ion acoustic waves in a quantized degenerate magnetoplasma with trapped electrons. Phys Plasmas 2015;22(2):022303.
[50] Shah HA, Iqbal M, Tsintsadze N, Masood W, Qureshi MNS. Effect of trapping in a degenerate plasma in the presence of a quantizing magnetic field. Phys Plasmas 2012;19(9):092304.
[51] Shah HA, Masood W, Asim M, Qureshi MNS. Drift solitary structures in inhomogeneous degenerate quantum plasmas with trapped electrons. Astrophys Space Sci 2014;350(2):615–22.
[52] Weiland J. Collective modes in inhomogeneous plasmas: kinetic and advanced fluid theory. CRC Press; 1999.